G. Aletti M. Burger A. Micheletti D. Morale
Editors

Math Everywhere

Deterministic and Stochastic Modelling
in Biomedicine, Economics and Industry.
Dedicated to
the 60th Birthday of Vincenzo Capasso

Springer

Structural Adaptation in Normal and Cancerous Vasculature

Philip K. Maini[1], Tomás Alarcón[2], Helen M. Byrne[3], Markus R. Owen[3], and James Murphy[3]

[1] Centre for Mathematical Biology, Mathematical Institute, University of Oxford, Oxford OX1 3LB, UK maini@maths.ox.ac.uk
[2] Bioinformatics Unit, Department of Computer Science, University College London, Gower Street, London WC1E 6BT, UK t.alarcon@cs.ucl.ac.uk
[3] Centre for Mathematical Medicine, School of Mathematical Sciences, University of Nottingham, Nottingham NG7 2RD, UK helen.byrne@nottingham.ac.uk, markus.owen@nottingham.ac.uk

Dedicated to Professor Vincenzo Capasso on the occasion of his 60th birthday

Summary. The dynamics of cancerous tissue growth involves the complex interaction of a number of phenomena interacting over a range of temporal and spatial scales. While several processes involved have been studied, the adaptation of the vasculature within a growing tumour has thus far received little attention. We consider a hybrid cellular automaton model which analyses the interaction between the tumour vascular network and tissue growth. We compute the temporal behaviour of the cancerous cell population under different hypotheses of structural adaptation in the vasculature. This may provide a possible method of determining experimentally which adaptation mechanisms are at work.

1 Introduction

The main function of vasculature is to ensure adequate and efficient nutrient delivery to tissue. To achieve this, blood vessels must be able to structurally adapt in response to signals from the tissue they perfuse. Experimental and theoretical studies have significantly advanced our understanding of the possible design principles and adaptation mechanisms at work in normal vessels [7], but there are still many open questions, and how these aspects of vasculature design change under diseased or abnormal conditions largely remains a mystery.

In normal vasculature, design principles based on an optimality assumption were first proposed by Murray [8], whereby the structure of the vascular system is postulated to arise from the balance between blood metabolic energy

consumption and energy dissipated by blood flow. Murray's design principle has been shown to imply that the wall shear stress (WSS) must be constant over the vascular network and experimental data appear to validate these predictions for arteries [15]. However, more recent experimental studies by Pries et al. [10] have shown that the WSS is not constant in smaller arterioles and capillaries, thus contradicting these predictions. Based on these results, they proposed a design principle whereby the vascular system must adapt to a sigmoidal WSS-pressure curve. A design principle based on Murray's optimality principle and recent blood-rheological data [3] has been shown to reproduce the non-constant WSS-pressure relationship found by Pries et al. [10].

Adaptation of the normal vascular system to a number of stimuli has been extensively analysed by Pries et al. [11, 12]. They have considered a model which accounts for adaptation in response to haemodynamic signals (WSS and pressure [13]) and metabolic stimulus, and have also considered both upstream and downstream signalling between vessels. The actual mechanistic bases for these stimuli are largely unknown, although there is some evidence that the downstream signal is carried by ATP molecules, whereas the upstream signal consists of changes in the membrane potential of endothelial cells that are propagated along the vessel walls.

In contrast to normal vasculature, which appears well organised according to the principles mentioned above, tumour vasculature appears to be very disorganised in all respects. Vessels lack the well-defined anatomical structure of their normal counterparts and are leaky. Blood flow in tumour vascular beds is also quite disorganised compared to normal circulation. In addition, there is evidence of signalling between tumour cells and normal vessels that induces a dematuration process within normal vessels as tumour malignancy progresses and co-opts normal vessels [14]. The significance of understanding how these changes affect circulation is obvious when one considers that the vasculature delivers drugs to the tumour.

In a first attempt towards a model of tumour vasculature, we aim to assess which of the normal adaptation mechanisms are more likely to be absent in tumour vasculature. To this end, we use the multi-scale model framework proposed in [2] to assess the effects of different adaptation cues. In effect, we "turn off" individual elements of the normal adaptation mechanism proposed by Pries et al. [12] and determine predicted outcomes. We hope that by experimental observation of tumour dynamics, one might then be able to deduce what structural adaptation mechanisms are at work.

2 Summary of the Multi-scale Model

The model we use integrates phenomena occurring on very different time and length scales TLSs (see Fig. 1). These features include blood flow and structural adaptation of the vascular network, transport into the tissue of

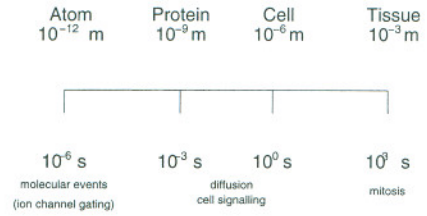

Fig. 1: Time and length scales involved in our model [6].

blood-borne oxygen, competition between cancer and normal cells, cell division, apoptosis, VEGF (growth factor) release, and the coupling between them. In this section we present an overview of the main features of the integrated model without entering into a detailed description of the sub-models which form its component parts.

The modelling framework we use is based on the hybrid cellular automaton concept which has been used to model several aspects of tumour development (see [1, 5, 9]). We extend this approach to account not only for the presence of a diffusive substance (such as oxygen or glucose) as in previous papers, but also to include intracellular and tissue-scale phenomena, and the coupling between them. To this end, we have organised our model into three layers: vascular, cellular, and intracellular, which correspond, respectively, to the tissue, cellular and intracellular TLSs, (see Fig. 2). For a full account of the details we refer the reader to [2].

In the top layer, we deal with the structure of the vascular network and blood flow (see [1] for more details). We consider a hexagonal vascular network (similar to the one observed in liver). Each individual vessel is assumed to undergo structural adaptation (i.e. changes in radius) in response to different stimuli until the network reaches a quasi-equilibrium state. Through this structural adaptation process we compute the blood flow rate, the pressure drop and the haematocrit (i.e. relative volume of red blood cells) distribution in each vessel. Between the vascular layer and the cellular layer, i.e. coupling the dynamics at the cellular level to blood flow and vascular adaptation, we have the transport of blood-borne oxygen into the tissue. This process is modelled by a reaction-diffusion equation. The distribution of haematocrit is the source of oxygen, whereas the distribution of cells (provided by the cellular layer) gives us the (spatially distributed) sink of oxygen.

In the intermediate layer, we focus on cell-cell interactions (competition) and spatial distribution of cells. We consider two types of cells: normal and cancerous, which are modelled as individual elements. These two populations compete for space and resources. Cancerous phenotypes are usually better competitors, which results in the cancer population taking over. Competition between the two types of cells is introduced by a very simple rule, which, in turn, couples this middle layer to the intracellular layer. Apoptosis

(programmed cell death) is controlled by the expression of p 53 (whose dynamics is dealt with in the intracellular layer): when the level of p 53 in a cell exceeds some threshold the cell undergoes apoptosis. However, this threshold is fixed according to the local spatial distribution of cells, which links the spatial distribution (cellular layer) with the apoptotic process (intracellular layer).

In the bottom layer, we consider intracellular processes, in particular cell division, apoptosis, and VEGF secretion. In this layer, we use ordinary differential equations (ODEs) to model the relevant biochemistry. One issue we focus on is how the external conditions modulate the dynamics of these intracellular phenomena and, in particular, how the level of extracellular oxygen affects the division rate, the expression of p 53 (which regulates apoptosis) and the production of VEGF. Since the spatial distribution of oxygen depends on both the spatial distribution of cells (cellular layer) and on the distribution of haematocrit (vascular layer), these processes at the intracellular level are linked to the behaviour of the other two layers: cell proliferation and apoptosis alter the spatial distribution of the cells (see Fig. 2); the cellular and the intracellular layers modulate the process of vascular structural adaptation through another transport process: diffusion of VEGF into the tissue and its absorption by the endothelial cells (ECs) lining the vessels.

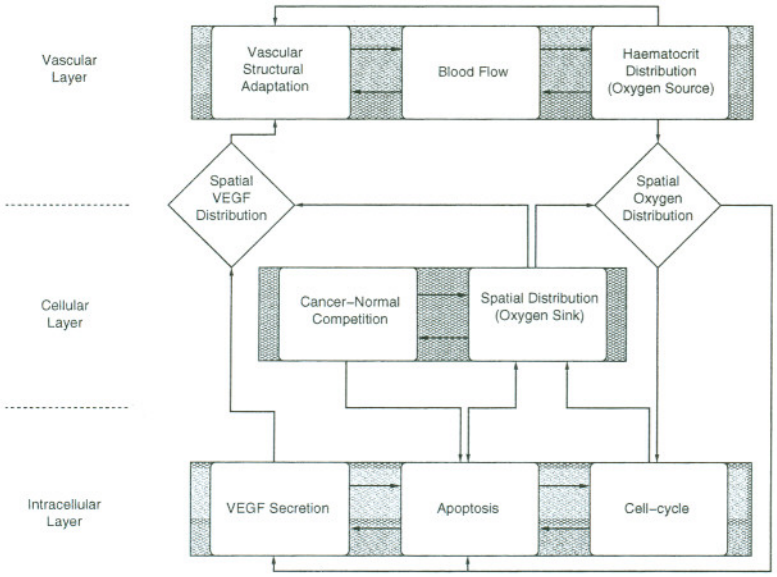

Fig. 2: Diagrammatic representation of the layer structure of our model.

3 Structural Adaptation in Normal Vasculature

In a series of papers, Pries, Secomb and co-workers have put together a model for vascular structural adaptation [11, 12]. According to this model, structural adaptation in normal vasculature occurs by adapting vessel radii to different stimuli:

$$\Delta R = S_{\text{tot}} R \Delta t$$

where R is vessel radius, Δt the time step, and S_{tot} is the total stimulus, given by the sum of the different stimuli. According to [11], there are three types of stimuli, and we briefly describe each one in turn. They assume a *haemodynamic* stimulus, which forces the vessels to adapt to blood flow conditions. The main signals involved in haemodynamic adaptation appear to be wall shear stress, τ_w, and pressure, P [13], although each of these magnitudes seems to play a different role: whereas increased WSS generally induces radius increase, increased pressure leads to decrease in vessel radius [12]. Accordingly, Pries et al. [12] postulate the following form for the haemodynamic stimulus, S_{h}:

$$S_{\text{h}} = \log(\tau_w + \tau_r) - k_p \log(\tau_e(P))$$

where τ_r is a constant introduced to avoid singular behaviour for low WSS, k_p is a constant and $\tau_e(P)$ is the level of WSS expected from the actual value of the intravascular pressure [12].

The second stimulus is the so-called *metabolic* stimulus. It is well known that, as part of their normal functionality, vessels respond and adapt to the metabolic needs of the surrounding tissue. Pries et al. [11] considered the following functional form for the metabolic stimulus, S_{m}:

$$S_{\text{m}} = k_m \log\left(1 + \frac{\dot{Q}_r}{\dot{Q}H}\right) \tag{1}$$

where k_m is a constant, $\dot{Q}_r$ is a reference blood flow and H is the haematocrit. In [2], a modification of Eq. (1) was proposed in order to explicitly take into account the effect on the vasculature of VEGF, V (produced by nutrient-deprived cells) whereby the constant k_m was replaced by a function of V:

$$k_m(V) = k_m^0\left(1 + \frac{V}{V_0 + V}\right) \tag{2}$$

where k_m^0 and V_0 are constants.

The third stimulus is actually a pair of stimuli, the so-called *conducted* stimuli, which consist of signals generated by the vessels and propagate either downstream or upstream. They are assumed to be necessary to maintain a fully functional vascular system. These signals are usually emitted under stress conditions, and therefore are closely related to the metabolic stimulus

described above. Although most of the underlying biological details of these signalling mechanisms are unknown, the downstream stimulus is hypothesised to be transmitted by a chemical which is released into the blood (a good candidate seems to be ATP released by red blood cells under hypoxic conditions [4]) and thereby carried downstream by the flow. The upstream transmission of information seems to be along the vessel walls, perhaps by spread of changes in membrane potential through gap junctions [12].

4 Deconstructing Normal Vasculature

We now examine, in turn, the effect on tumour cell population dynamics of these stimuli. Specifically, we focus on those stimuli which are most likely to be absent in tumour vascular networks.

4.1 Adaptation Decoupled from VEGF Production

For completeness and later comparison, we first carry out simulations with $k_m = k_m^0$ independent of VEGF in Eq. (1). No conducted stimuli are introduced, so S_{tot} is given by:

$$S_{\text{tot}} = S_{\text{h}} + S_{\text{m}} - k_s$$

where k_s is the so-called *shrinking tendency* which accounts for vessel shrinkage in the absence of stimuli [11].

The results obtained are shown in Fig. 3. As we can see, the growth of the tumour does not have any impact on the vascular network, as tumour growth and vascular adaptation are effectively decoupled. It is worth noting the formation of a necrotic core in the centre of the growing tumour. We see that the flow is evenly distributed along the pathways running parallel to the diagonal as a consequence of the boundary conditions which are flow inward at the bottom left-hand corner, flow outward at the top right-hand corner, and zero flux elsewhere.

4.2 Adaptation Coupled to VEGF Production

We now account for the coupling between vasculature and VEGF, by taking in Eq. (1) $k_m = k_m(V)$ as given by Eq. (2). No conducted stimuli are introduced, so S_{tot} is given by:

$$S_{\text{tot}} = S_{\text{h}} + S_{\text{m}} - k_s.$$

In this case (see Fig. 4) the behaviour of the system resembles more closely what we would expect in a tumour: there are extensive hypoxic regions within the tumour, but no noticeable necrotic regions. We also see that this model, as

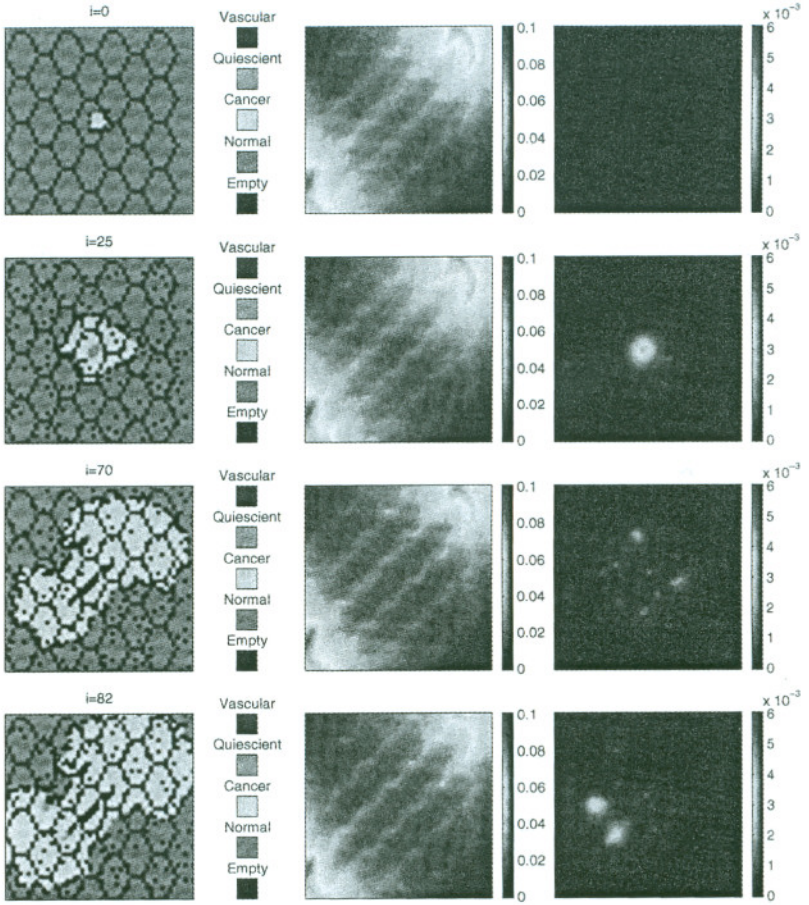

Fig. 3: Four snapshots showing simulations with no VEGF coupling and no conducted stimuli. Time increases from top to bottom. The left column corresponds to the evolution of the colonies of normal and cancerous cells, the central column to the distribution of oxygen and the right column to VEGF distribution. See also Plate 4 on page 339

in the previous case, leads to parallel circulatory pathways running along the diagonal. However, in this case, due to the coupling between VEGF production and vascular adaptation, there is only one pathway that takes most of the flow. This continues until eventually an instability occurs whereby there is basically only one pathway that carries all the flow. This may well contribute to the dynamic and rather unstable spatial patterns formed by real tumours.

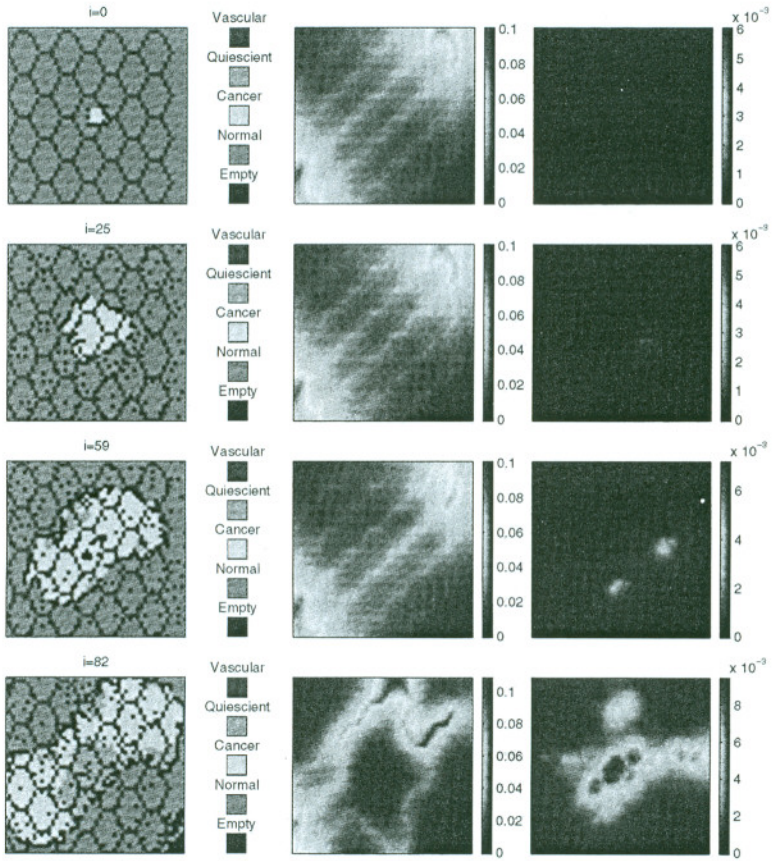

Fig. 4: Four snapshots showing simulations with vascular adaptation coupled to VEGF released by hypoxic cells. Time increases from top to bottom. The left column corresponds to the evolution of the colonies of normal and cancerous cells, the central column to the distribution of oxygen and the right column to VEGF distribution. See also Plate 5 on page 340

4.3 Inclusion of Downstream Signalling

The mechanism we propose for downstream transmission of signals differs somewhat from that proposed by Pries et al. [12]. Whereas they consider that the downstream stimulus is long-range and propagates from any vessel of the network to any other vessel downstream of it, we will assume that the downstream stimulus is only transmitted to the nearest neighbour, i.e. to the vessels immediately downstream of the one releasing the signal. The mechanism proposed by Pries et al. [12] relies on the fact that the chemical carrying the signal has a long half-life time in blood, which allows it to stay in the circulation for a significant length of time. Our mechanism, on the contrary, is based on the assumption that the chemical has a short half-life time. Because the identity and properties of the actual chemical are unknown, both mechanisms are feasible *a priori*.

The intensity of the downstream stimulus, S_{d}, is assumed to depend on the current of the signalling chemical along a particular vessel (vessel "1", say). If the vessels upstream (vessels "2" and "3") of vessel 1 are irrigating hypoxic regions, they will be receiving signals from the tissue in the form of secreted VEGF. If this is the case, i.e. if the concentration of VEGF in any of the vessels 2 or 3 is larger than zero, then these vessels will produce a (constant) amount of signalling chemical, ρ_0. The chemical produced in vessels 2 and 3 will enter vessel 1 and its current along vessel 1 will be (due to mass conservation):

$$J_1 = \rho_1(V)\dot{Q}_2 + \rho_2(V)\dot{Q}_2$$

where $\rho_i(V) = \rho_0$ if $V \neq 0$ in vessel $i = 1, 2$ and $\rho_i(V) = 0$ if $V = 0$ in vessel $i = 1, 2$. Using now the formula given in [12], S_{d} is given by:

$$S_{\mathrm{d}} = \log\left(1 + \frac{J_1}{\dot{Q} + \dot{Q}_{ref}}\right)$$

where $\dot{Q}_{ref}$ is a constant introduced to avoid singular behaviour. The total stimulus is then given by

$$S_{\mathrm{tot}} = S_{\mathrm{h}} + S_{\mathrm{m}} + S_{\mathrm{d}} - k_s$$

with $k_m = k_m(V)$ as in Eq. (2), i.e. the coupling between vascular adaptation and VEGF production is taken into account.

The corresponding results are shown in Fig. 5. Comparing the results to those obtained in Section 4.2, we see that this vasculature yields tumours with smaller hypoxic regions which release lower concentrations of VEGF. Related to this behaviour, we also observe differences in the vasculature and blood flow with respect to the two previous cases (Sections 4.1 and 4.2). In this case, the flow is initially distributed within disconnected pathways along the diagonal, but eventually blood flow is established along paths connecting

the diagonal pathways (which are still the main flow paths). This generates a more homogeneous pattern of blood flow and oxygen concentration which leads to smaller hypoxic regions and therefore to a much more stable spatial pattern.

Therefore the inclusion of "first-neighbour" downstream signalling yields a more "normal-looking" vasculature and more static spatial pattern within the tumour. This leads to the conclusion that this mechanism of vascular adaptation is quite likely to be absent in tumour circulation.

4.4 Inclusion of Upstream Signalling

Following Pries et al. [12], the intensity of the upstream stimulus, S_{u}, is assumed to depend on a signal produced by vessels in hypoxic regions ($V > 0$). The "amount" of signal produced is assumed to be proportional to the length of the vessel, L_s. As in [12], we further assume the existence of a dissipative mechanism in the upstream signal propagation, which will be modelled by an exponential decay. At a given node of the network, the current of upstream stimulus produced by each "outgoing" vessel (defined as one such that the corresponding current has a negative value) is given by:

$$J_c^o = L_s \mathrm{e}^{-L_s/L}$$

where L is a constant.

The total current, J_c, is the sum over all the outgoing vessels at a given node of the corresponding values of J_c^o. The upstream stimulus at each of the incoming vessels at the corresponding node is given by [12]:

$$S_{\mathrm{u}} = k_m k_c \frac{J_c}{J_c + J_0}$$

where J_0 is a constant. The total stimulus is then given by

$$S_{\mathrm{tot}} = S_{\mathrm{h}} + S_{\mathrm{m}} + S_{\mathrm{u}} - k_s.$$

Typical results are shown in Fig. 6. Comparing the results to those obtained in Section 4.3, we see that this mechanism yields a vasculature in which the circulation is heavily concentrated around the regions under hypoxic stress, in contrast to the situation observed in Fig. 5, in which the action of the downstream stimulus tends to homogenise the pattern of flow. The way in which this flow concentration around hypoxic regions is achieved is different from the one shown in Fig. 4, corresponding to an adaptation mechanism without long-range stimuli. In Fig. 4 we see that when several hypoxic regions appear within the tumour mass the adaptation mechanism reacts by creating large parallel vessels running through the hypoxic regions from inlet to outlet. In the present case (see Fig. 5), the pattern of flow when a number of hypoxic regions appear is much more homogeneous and "normal looking". Therefore we suggest that this mechanism is quite likely to be absent in tumour vasculature.

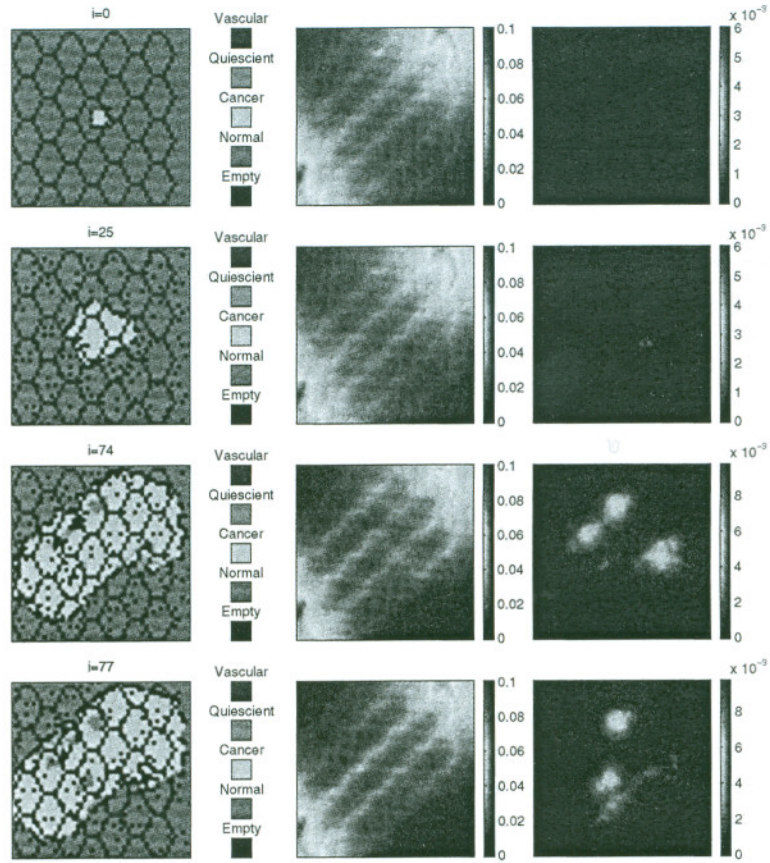

Fig. 5: Four snapshots showing simulations with a structural adaptation mechanism coupled to VEGF released by hypoxic cells plus "nearest-neighbour" downstream stimulus. The left column corresponds to the evolution of the colonies of normal and cancerous cells, the central column to the distribution of oxygen and the right column to VEGF distribution. See also Plate 6 on page 341

5 Conclusions and Discussion

We have used a previously developed hybrid cellular automaton model to explore the effects on tumour cell dynamics of different vasculature structural adaptation mechanisms. We summarise our new results as follows:

- Only vasculature in which adaptation is decoupled from VEGF can support a necrotic core, with a size which appears to correlate with total

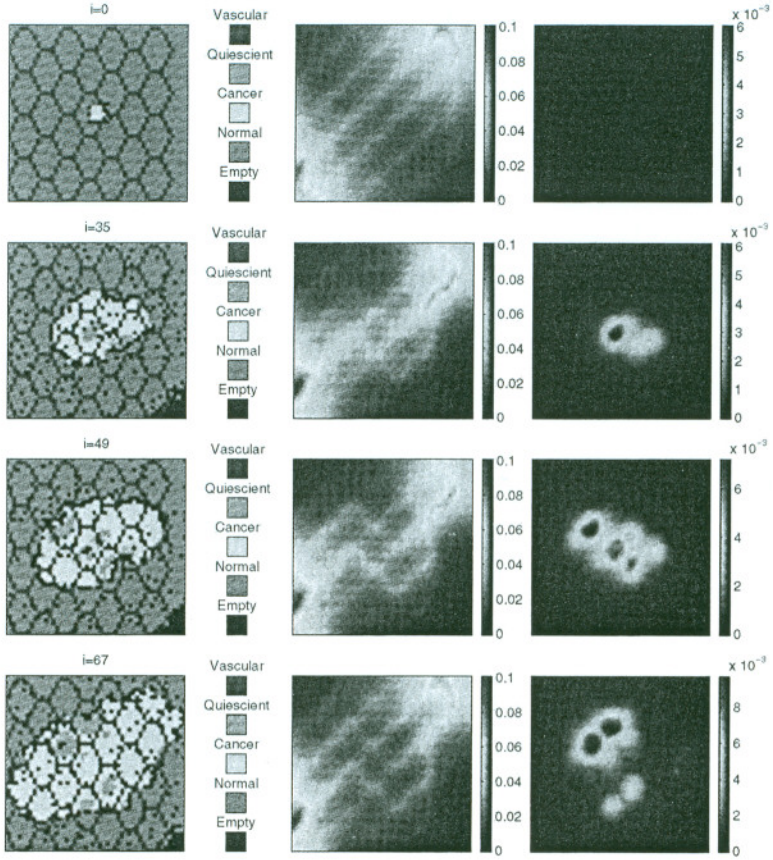

Fig. 6: Four snapshots showing simulations with a structural adaptation mechanism coupled to VEGF released by hypoxic cells plus "nearest-neighbour" upstream stimulus. The left column corresponds to the evolution of the colonies of normal and cancerous cells, the central column to the distribution of oxygen and the right column to VEGF distribution. See also Plate 7 on page 342

tumour size (see Fig. 3). This is due to the inability of the tumour to induce sufficient vasculature to supply extra oxygen to that particular region.

- The vasculature generated by assuming coupling between vascular adaptation and VEGF production appears to produce the most spatially heterogeneous pattern of flow and oxygen. Eventually the system evolves to one pathway carrying almost all of the flow.

- When introducing nearest-neighbour downstream signalling, the distribution of flow and oxygen becomes more homogeneous, yielding a much more stable spatial pattern within the tumour.
- Upstream signalling yields concentration of flow and oxygen around the hypoxic regions, although the patterns of flow look much more homogeneous than in the case without downstream and upstream stimuli.
- The size of hypoxic regions appears to correlate with the homogeneity of flow and oxygen distributions. Heterogeneous distributions (Fig. 4) yield larger hypoxic regions.

While in the above we have compared spatial distributions of key components in response to different stimuli, we can also easily compute how the total number of cells changes over time. In Fig. 7 we observe how the total number of cells and their temporal dynamics depend quite critically on the adaptation mechanism assumed. Intriguingly, the model predicts oscillatory behaviour in cancerous cell population.

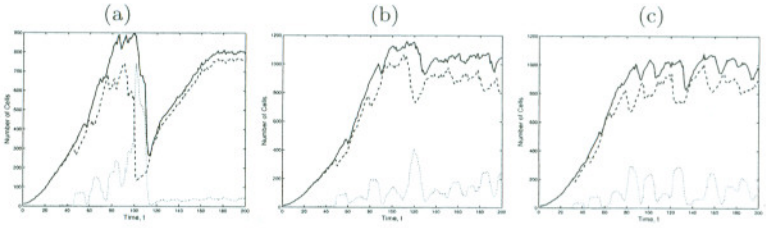

Fig. 7: Number of cells as a function of time for the different vascular adaptation mechanisms considered. Panel (a) shows the results for a VEGF-sensitive vasculature with no conducted stimuli. Panels (b) and (c) incorporate, in addition to VEGF coupling, downstream stimulus and upstream stimulus, respectively. Key: solid line corresponds to the total number of cancerous cells (quiescent plus proliferating), dashed line to the number of proliferating cancerous cells and dotted line to the number of quiescent cancerous cells.

There are many future directions in which this preliminary work must be extended to capture more realistically the biology of vasculature adaptation and cancerous cell dynamics. For example, the approach that we have used is based on empirical evidence of structural adaptation in large vessels. It is unclear if this holds in general for blood vessels. We will need to develop an adaptation principle which is more mechanistically based, allowing it to be verified more easily experimentally. However, the present study has yielded a number of experimentally testable predictions which may help elucidate some of the key underlying processes of adaptation which are absent or work abnormally in tumour vasculature.

Acknowledegments

TA would like to thank the EPSRC for financial support (grant GR/509067).

References

1. T. Alarcón, H.M. Byrne, P.K. Maini. *A cellular automaton model for tumour growth in a heterogeneous environment.* J. theor. Biol. **225**, 257–274 (2003).
2. T. Alarcón, H.M. Byrne, P.K. Maini. *A multiple scale model for tumour growth.* SIAM Multiscale Model. Simul. **3**, 440–475 (2005).
3. T. Alarcón, H.M. Byrne, P.K. Maini. *A design principle for vascular beds: The effects of complex blood rheology.* Microvasc. Res. **69**, 156–172 (2005).
4. D.M. Collins, W.T. McCullough, M.L. Ellsworth. *Conducted vascular responses: Communication across the capillary bed.* Microvasc. Res. **56**, 43–53 (1998).
5. A. Deutsch, S. Dormann. *Modeling of avascular tumor growth with a hybrid cellular automaton.* In Silico Biol. **2**, 1–14 (2002).
6. P.J. Hunter, P. Robbins, D. Noble. *The IUPS human physiome project.* Pflügers Archiv- Eur. J. Physiol. **445**, 1–9 (2002).
7. M. LaBarbera. *Principles of design of fluid transport systems in zoology.* Science. **249**, 992–1000 (1990).
8. C.D. Murray. *The physiological principle of minimom work I The vascular system and the cost of blood volume.* Proc. Nat. Acad. Sci. USA. **12**, 207 (1977).
9. A.A. Patel, E.T. Gawlinski, S.K. Lemieux, R.A. Gatenby. *A cellular automaton model of early tumor growth and invasion: The effects of native tissue vascularity and increased anaerobic tumor metabolism.* J. theor. Biol. **213**, 315–331 (2001).
10. A.R. Pries, T.W. Secomb, P. Gaehtgens. *Design principles of vascular beds.* Circ. Res. **77**, 1017–1023 (1995).
11. A.R. Pries, T.W. Secomb, P. Gaehtgens. *Structural adaptation and stability of microvascular networks: theory and simulations.* Am. J. Physiol. **275**, H349–H360 (1998).
12. A.R. Pries, B. Reglin, T.W. Secomb. *Structural adaptation of microvascular networks: functional response to adaptive responses.* Am. J. Physiol. **281**, H1015–H1025 (2001).
13. N. Resnick, H. Yahav, A. Shay-Salit, M. Shushy, S. Schubert, L.C.M. Zilberman, E. Wofovitz. *Fluid shear stress and the vascular endothelium: for better and for worse.* Progress Biophys. Mol. Biol. **81**, 177–199 (2003).
14. G.D. Yancopoulos, S. Davis, N.W. Gale, J.S. Rudge, S.J. Wiegand, J. Holash. *Vascular-specific growth factors and blood vessel formation.* Nature. **407**, 242–248 (2000).
15. M. Zamir. *Shear forces and blood vessel radii in vardiovascular-system.* J. Gen. Physiol. **69**, 449–461 (1977).

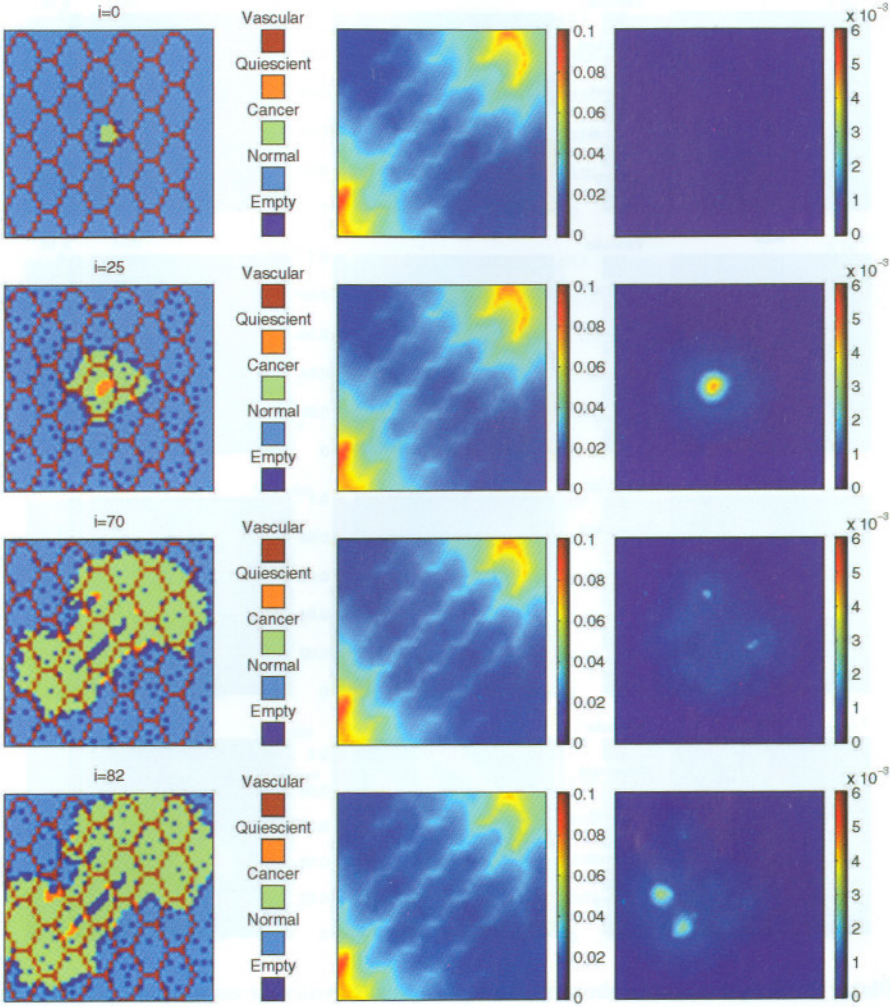

Plate 4: Four snapshots showing simulations with no VEGF coupling and no conducted stimuli. Time increases from top to bottom. The left column corresponds to the evolution of the colonies of normal and cancerous cells, the central column to the distribution of oxygen and the right column to VEGF distribution (*P.K. Maini et al., Figure 3 page 171*)

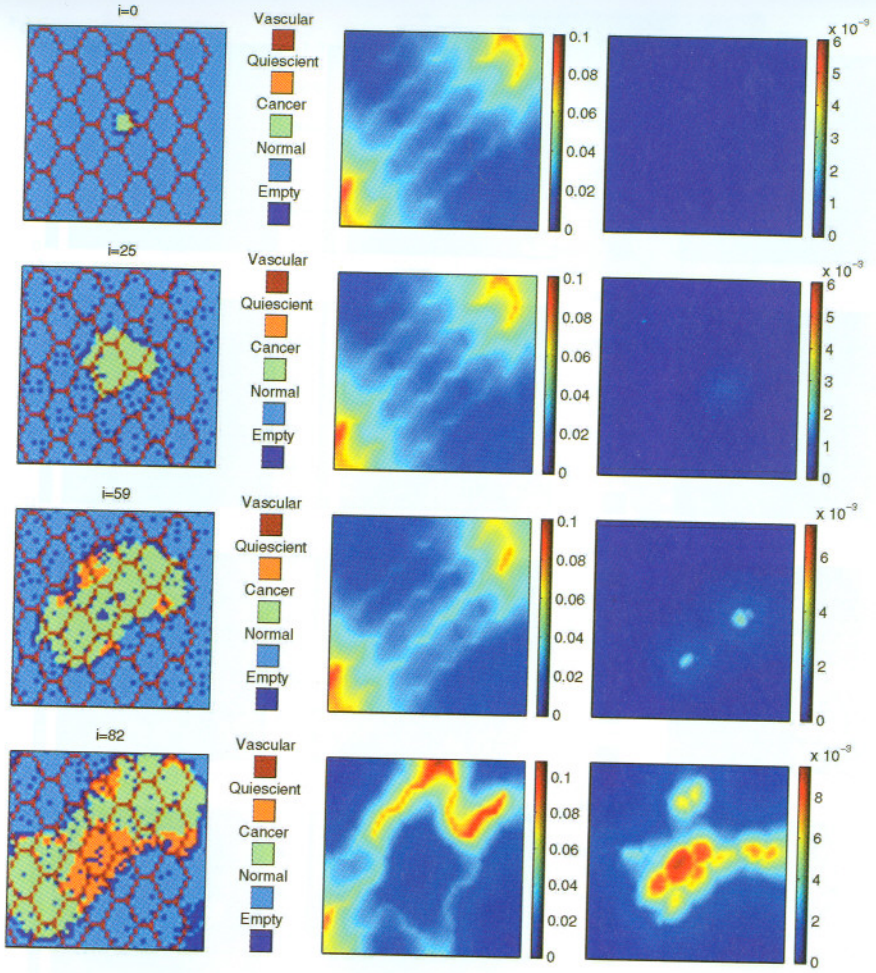

Plate 5: Four snapshots showing simulations with vascular adaptation coupled to VEGF released by hypoxic cells. Time increases from top to bottom. The left column corresponds to the evolution of the colonies of normal and cancerous cells, the central column to the distribution of oxygen and the right column to VEGF distribution (*P.K. Maini et al., Figure 4 page 172*)

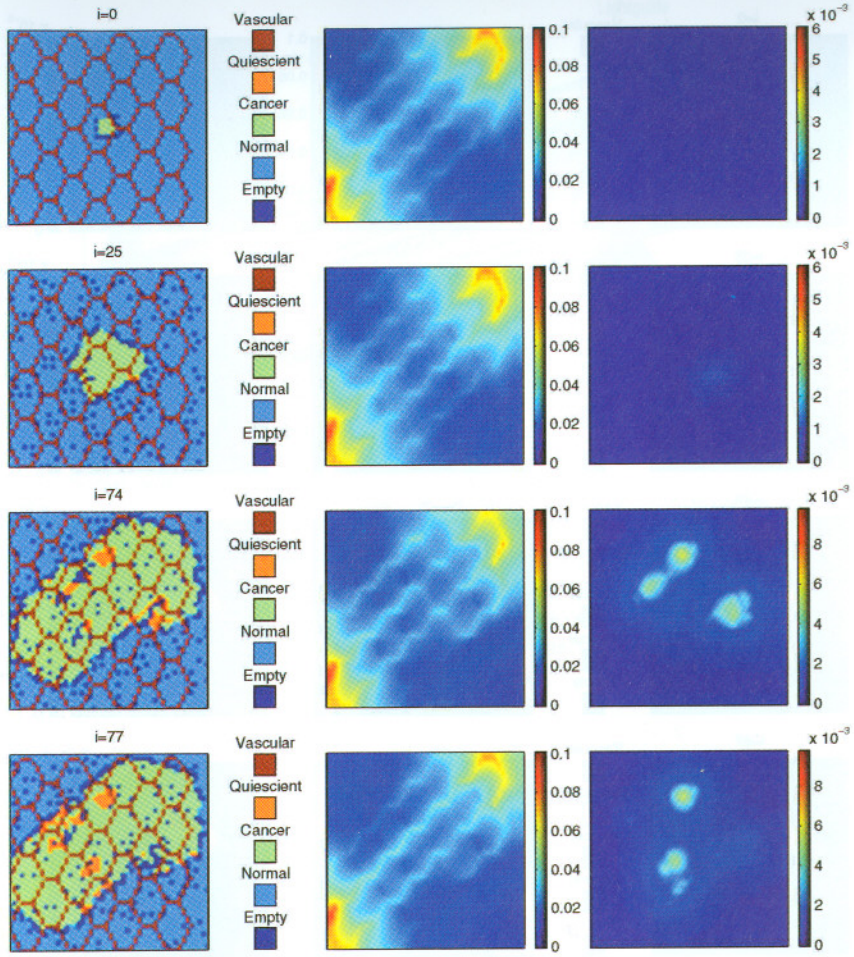

Plate 6: Four snapshots showing simulations with a structural adaptation mechanism coupled to VEGF released by hypoxic cells plus "nearest-neighbour" downstream stimulus. The left column corresponds to the evolution of the colonies of normal and cancerous cells, the central column to the distribution of oxygen and the right column to VEGF distribution (*P.K. Maini et al., Figure 5 page 174*)

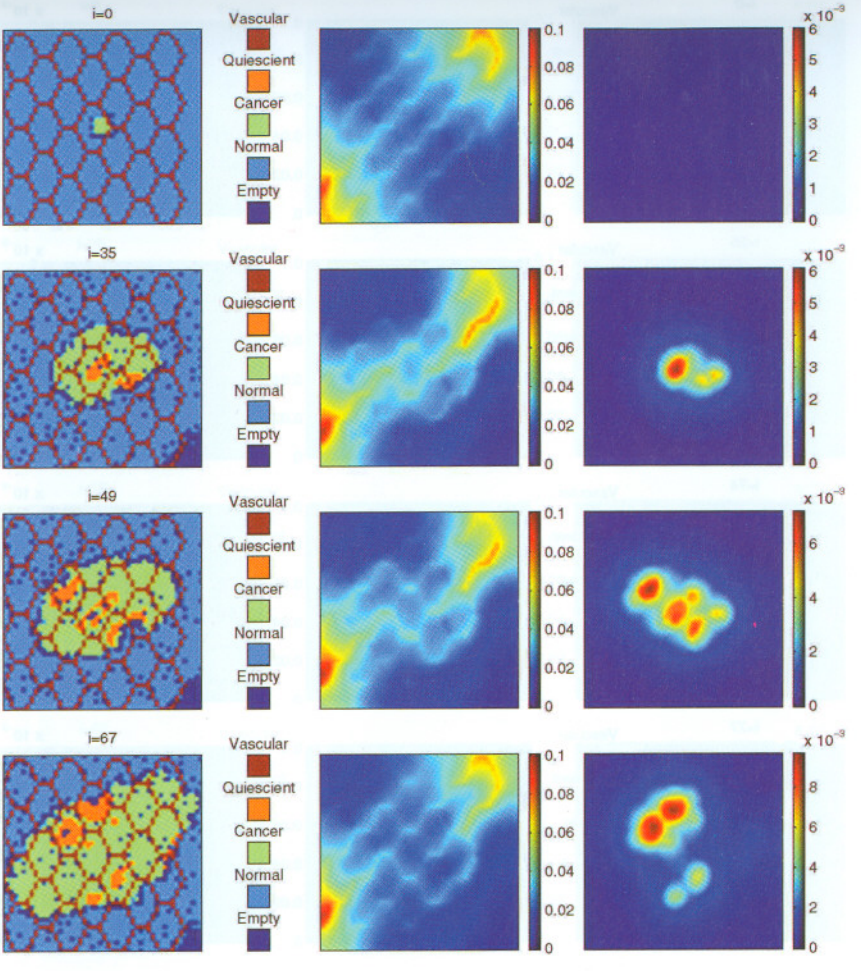

Plate 7: Four snapshots showing simulations with a structural adaptation mechanism coupled to VEGF released by hypoxic cells plus "nearest-neighbour" upstream stimulus. The left column corresponds to the evolution of the colonies of normal and cancerous cells, the central column to the distribution of oxygen and the right column to VEGF distribution (*P.K. Maini et al., Figure 6 on page 176*)